Journal of Theoretical Biology 534 (2022) 110947

Contents lists available at ScienceDirect

Journal of Theoretical Biology

journal homepage: www.elsevier.com/locate/yjtbi

Model of drug delivery to populations composed of two cell types

Sid Becker [a,*], Andrey V. Kuznetsov [b], Dan Zhao [a], Filippo de Monte [c], Giuseppe Pontrelli [d]

[a] University of Canterbury, Department of Mechanical Engineering, Christchurch, New Zealand
[b] Department of Mechanical and Aerospace Engineering, North Carolina State University, Raleigh, NC, USA
[c] Department of Industrial and Information Engineering and Economics, University of L'Aquila, L'Aquila, Italy
[d] Istituto per le Applicazioni del Calcolo (IAC), CNR, Rome, Italy

ARTICLE INFO

Article history:
Received 2 July 2021
Revised 20 October 2021
Accepted 22 October 2021
Available online 27 October 2021

Keywords:
Pharmacokinetic
Three compartment
Drug delivery
Continuum
Macroscale
Porous
Chemotherapy
Michaelis-Menten reaction
Transport
Binding model

ABSTRACT

The rate of drug delivery to cells and the subsequent rate of drug metabolism are dependent on the cell membrane permeability to the drug. In some cases, tissue may be composed of different types of cells that exhibit order of magnitude differences in their membrane permeabilities. This paper presents a brief review of the components of the tissue scale three-compartment pharmacokinetic model of drug delivery to single–cell–type populations. The existing model is extended to consider tissue composed of two different cell types. A case study is presented of infusion mediated delivery of doxorubicin to a tumor that is composed of a drug reactive cell type and of a drug resistive cell type. The membrane permeabilities of the two cell types differ by an order of magnitude. A parametric investigation of the population composition is conducted and it is shown that the drug metabolism of the low permeability cells are negatively influenced by the fraction of the tissue composed of the permeable drug reactive cells. This is because when the population is composed mostly of drug permeable cells, the extracellular space is rapidly depleted of the drug. This has two compounding effects: (i) locally there is simply less drug available to the neighboring drug resistant cells, and (ii) the depletion of the drug from the extracellular space near the vessel-tissue interface leaves less drug to be transported to both cell types farther away from the vessel.

1. Introduction

The compartment pharmacokinetic model is used in pharmacological studies to describe the delivery and transport of molecules to tissues and cell cultures (Jackson, 2003; Groh et al., 2014; Clarelli et al., 2020; Dordal et al., 1995; Eikenberry, 2009). This family of models has been used almost exclusively for single–cell–type populations. It is well understood that in some chemotherapeutic treatments, however, different types of cells may react differently to the drug. Examples occur in the treatment of tissues that are composed of both healthy and cancerous cells, or in the treatment of tissue composed of both drug resistant and drug responsive cells. The biophysical characteristics of the cell membrane have been associated with the drug resistivity of cancer cells (Ferté, 2000). The mechanical properties of the cell membrane in cancer cells have been demonstrated to play a role in the sensitivity/resistivity to the anticancer drug doxorubicin (DOX) (Bell et al., 2013). A recent experimental study showed that the cell wall model characteristics associated with healthy cells had an apparent permeability to DOX that was an order of magnitude higher compared to that of a cell wall associated with cancerous cell conditions (Aminipour et al., 2020). In the study (Peetla et al., 2010) the authors show that cell lines that are that are resistant to DOX show a lower transmembrane permeability than the cells that are sensitive to the drug.

1.1. Single–Cell–Type population compartment models

Pharmacological continuum models that depict mass transfer from the extracellular space (EC) to the cell interior often use the concept of binding (Clarelli et al., 2020; Lauffenburger and Linderman, 1993; McGinty and Pontrelli, 2016). Within the EC, the drug is free to diffuse and interact with its environment; this is the drug's unbound state (or free state). The drug molecule is designed to reach specific receptors on the cell membrane or within the cell cytosol. These are referred to as specific binding sites; the drug that is bound to these sites is considered to be in its specific bound state. Sometimes the molecule may instead interact with unintended receptors or other molecules so that the drug is unable to reach the intended receptors. In this case,

* Corresponding author.
E-mail address: sid.becker@canterbury.ac.nz (S. Becker).

https://doi.org/10.1016/j.jtbi.2021.110947
0022-5193/

the drug molecule would be considered to be in its non-specific bound state.

Many theoretical studies of drug delivery to cells use a three compartment model that represents the drug in three distinct phases: (i) the drug in the extracellular space, (ii) the drug in the intracellular space, and (iii) the product of reaction of the drug within the cell (Jackson, 2003; Groh et al., 2014; Clarelli et al., 2020; Dordal et al., 1995). Drug transport throughout the EC occurs by diffusion (and in some cases by slow advection). The cell membrane regulates the rate of transmembrane transport of the drug between the EC and the intracellular space. Only once it has entered the cell is the drug able to react with the intended internal receptors (resulting here in a product of reaction). A conceptual depiction of the 3 phases of the three-compartment model is presented in Fig. 1.

The mathematical expressions governing the conservation of drug in the three-compartment model represent the drug in its three states is represented by the coupled system of equations:

$$\begin{aligned}\frac{\partial C_{EC}}{\partial t} &= \nabla\cdot\mathbf{J}(C_{EC}) - F_{EC-I}(C_{EC},C_I)\\ \frac{\partial C_I}{\partial t} &= F_{I-EC}(C_{EC},C_I) - R(C_I,P_I)\\ \frac{\partial P_I}{\partial t} &= R(C_I,P_I).\end{aligned} \tag{1}$$

Here C_{EC} and C_I are the extracellular and intracellular drug concentrations, respectively, and P_I represents the intracellular concentration of the product of reaction. The drug flux within the EC, $\mathbf{J}(C_{EC})$, may be representative of simple diffusion, of advection resulting from some interstitial flow velocity, $\mathbf{v}$, or of a combination of the two. In the study that follows only diffusion mediated transport is considered.

The principal aim of drug delivery is to initiate some internal reaction within the cell . This requires that the drug passes the cell membrane, and the nature of transport across the cell wall is varied and molecule specific (Yang and Hinner, 2015). The function F_{EC-I} of Eq. (1) represent the transmembrane transport of the drug between from the extracellular space to the intracellular space (and F_{I-EC} represents the reverse). When the intrinsic drug concentrations are used, these functions must account for the difference in the volumes of the intracellular space and of the extracellular space. In models of single–cell–type populations, when intrinsic drug concentrations are used, the function of transmembrane transport F_{EC-I} scales linearly to F_{I-EC} by the ratio of intracellular volume to extracellular volume. For many molecules, the transmembrane flux is well represented by Fickian diffusion in which the rate of flux is linearly proportional to the transmembrane concentration gradient (Jackson, 2003; Groh et al., 2014; Clarelli et al., 2020; Dordal et al., 1995). For other molecules, the observed rate of transmembrane transport is saturable with respect to the transmembrane concentration gradient; when, for example, the transport is facilitated by a limited number of specialized carrier proteins (Yang and Hinner, 2015), continuum models often describe the rate of transfer in terms of Michaelis-Menten kinetics (Vendel et al., 2019; El-Kareh and Secomb, 2000; Vendel et al., 2019)

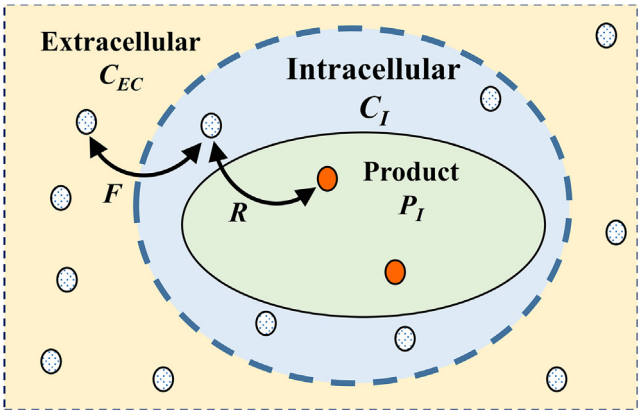

Fig. 1. The three compartment model in which the drug exists in three states: in its extracellular free state, in its intracellular free state, and as the intracellular product of reaction.

A conversion of the drug inside the cell to some product P_I may be described by a reaction, $R(C_I,P_I)$, that occurs between the drug and the internal organelles of the cell. In some cases the reaction is represented by an irreversible binding and the drug reaction rate is simply proportional to the concentration of the free drug in the cell cytosol (Jackson, 2003; Dordal et al., 1995). For many drugs, the relationship between the rate of targeted binding and the drug concentration is modeled in a non-linear reversible manner so that some of the bound drug may return to its free state. Many models describing these reactions often consider that the rate of the binding is limited by the number of available binding sites (Groh et al., 2014; Clarelli et al., 2020). Recent studies have accounted for both specific and nonspecific binding by including additional reaction terms (McGinty and Pontrelli, 2016; Chakravarty and Dalal, 2019).

Some compartmental models make the simplifying approximation that the transport across the cell wall is instantaneous (Clarelli et al., 2020; McGinty and Pontrelli, 2016; Vendel et al., 2019; Chakravarty and Dalal, 2019); here the internal and external concentrations of the drug in its free unbound state are equal $C_I = C_{EC} = C$. This local mass equilibrium approximation allows the three compartment model of Eqs. (1) to be represented by a two compartment model that does not distinguish between EC and IC drug concentrations:

$$\begin{aligned}\frac{\partial C}{\partial t} &= \nabla\cdot\mathbf{J}(C) - R(C,P)\\ \frac{\partial P}{\partial t} &= R(C,P).\end{aligned} \tag{2}$$

Because this representation fails to capture the time lag associated with the cell membrane's barrier function, this simplification should only be applied when the internal reactions occur on a much longer timescale than the transmembrane transport.

The representations of the compartmental model of drug delivery to cells in tissue are able to account for many different observed microscale phenomena, and while these theoretical models are able to conserve the drug mass in each of the phases, they consider only single–cell–type populations. It is reasonable to anticipate scenarios in which the tissues is composed of different cell types. For example when the cell membranes of healthy cells exhibit a higher permeability to the drug than the cell membranes of cancerous drug resistant cells. Such effects cannot be captured in models of single–cell–type populations.

1.2. Multiple cell population models

The motivation behind the current work is to present a model of drug transport to tissues or cell suspensions that are composed of multiple-cell-type populations: effectively to extend the general expression of Eq. (1) to include the conservation of drug in different cell types. In this section we review some of the applications of multiple–cell–type populations. While the models used in these applications do consider a domain composed of different types of cells, they do not explicitly conserve the drug (or chemical species) as is done in the 3 compartment representation of Eq. (1). These limitations are described next.

1.2.1. Tumor growth models

Depending on the application, algebraic, ordinary differential equations, and partial differential equations have been used to model tumor response to treatment and nutrient availability; a comprehensive list of the different models is provided in the first table of (Yin et al., 2019). The reaction–diffusion model (sometimes referred to in this context as the proliferation-invasion model) allows researchers to expand the analysis to consider spatio-temporal tumor behavior (Meghdadi et al., 2016; Preziosi et al., 2021). The review (Roose et al., 2007) presents different models of coupled sets of reaction–diffusion equations that account not only for the concentration of cancer cells, but also for the concentration of nutrients (upon which tumor growth is clearly dependent). The set accounts for the EC and the spaces occupied by different cell types. These models use conservative equations to represent the spatio-temporal changes in the volume fraction of each of these phases (Roose et al., 2007; Casciari et al., 1992). For each nutrient type, a diffusion–reaction equation may be used to represent the conservation of species (Roose et al., 2007; Byrne et al., 2003). Simplified representations of this system of equations include the two–phase system of (Ward, 1999) that considers only: (i) live cells and (ii) dead cells with the conservation of multiple nutrients. Another two–phase model is presented in (Breward et al., 2002) and modified by (Flegg and Nataraj, 2019) which considers the conservation of the two phases, (i) the cell phase and (ii) the extracellular fluid phase, and conserves the single nutrient, oxygen. These tumor-growth models have been developed to focus on the prediction of the distribution of tumor cell concentrations and not the conservation of the drug or chemical species in the different phase. The multiphase approach has been extended to different types of living cells (cancerous and normal cells for example). A drug resistance study by (Jackson and Byrne, 2000) modelled the diffusion of drug through a tumorous tissue composed of two types that respond differently to the drug. However that study did not account for the reduction of the drug mass in the EC resulting from the uptake of the drug by the cells; again this is because the focus of that study was the conservation of the cells and not of the drug.

1.2.2. Cell chemotaxis models

The uptake of some chemical species by multiple–cell–type populations has been represented in the continuum dynamics involved in the interaction between cell migration and the conservation of some chemical species. Chemotaxis, the tendency of a cell population to migrate in a preferential direction dependent on the concentration (or gradient in concentrations) of some chemical species is often represented by the Keller-Segel equation (Keller and Segel, 1971; Horstmann and From, 1970; Hillen and Painter, 2009). An interesting extension of this model is presented in the study by Ref. (Painter et al., 2000) that considers the chemotaxis of a single population of cells with two different chemical types. The model has also been adapted to include populations of more than one cell type; for the case of different cell types in competition for a chemical resource in (Stinner et al., 2014) and for the case when different cell types can interact with one another (Painter and Sherratt, 2003). These cell chemotaxis models are not developed to focus on the uptake of the chemical by the cell; these models are focused on the distribution and kinetics of the cellular concentrations. These models do not directly address the conservation of mass of the molecule taken up by the multiple cell types.

1.2.3. Viral dynamics models

The problem of the spreading of a virus has been considered in multiple–cell–type populations (Bocharov et al., 2018). Early models use coupled sets of ODE's that consider spatial uniformity in the transient behavior of three coupled expressions describing the dynamics of concertation of infected cells, non-infected cells, and virus (Nowak et al., 1996) and these employed the reaction kinetics similar to those described in the binding models. With further developments, diffusion related spatial effects were included in the model, initially to capture the 1D spread of a virus through a population of bacteria (Yin and McCaskill, 1992; You and Yin, 1999). These couple the concentration of the virus (which is free to diffuse through the extracellular media) to the concentration of uninfected cells and the concentration of infected cells. These models focus on the conservation of the number of cell types (infected or non-infected) and the virus is represented by a reaction rate (often nonlinear and irreversible), so that these models do not actually conserve the mass of the virus transferred to the cells.

2. Three compartment model of multi-cell-type populations

The models reviewed so far have considered the delivery of drugs to only a single–cell–type population, or if the models do consider a multiple–cell–type population, they do not conserve the drug (or species). In the sections that follow, we introduce a model of drug delivery to a region of tissue composed of different cell types and for which each cell type may respond differently to the drug administered. The extension of the three compartment model to a multiple–cell–type population is depicted in Fig. 2. Here C_{EC} is the intrinsic drug concentration in the EC. The intrinsic intracellular drug concentrations of Cell Type 1 and Cell Type 2 are C_1 and C_2, respectively. The products of reaction of the cell types are represented by the parameters P_1 and P_2. The mathematical representation require that each cell type be assigned its own unique transmembrane transport term and possibly its own unique reaction term(s). In the discussion that follows only the diffusion of drug in the extracellular space is considered and any advection resulting from some interstitial flow has been neglected.

2.1. Porosity, cell fraction, and drug concentration

The porosity of the tissue is the ratio of the volume occupied by the extracellular space, V_{EC}, to the total volume, V_T :

$$\varepsilon = \frac{V_{EC}}{V_T} = \frac{V_{EC}}{V_{EC} + V_C}. \tag{3}$$

Here V_C is the volume occupied by all cells. In this study the volume occupied by the cells comprises the volumes occupied by the two different cell types:

$$V_C = V_1 + V_2. \tag{4}$$

The fractions of the of the total number of cells that are of Type 1 and of Type 2 are represented by the parameters, $f_1 = n_1/n_C$ and $f_2 = n_2/n_C$. Under the approximation that the individual cell volume of the two cell types are equal, the fraction of cells of type 1 and type 2 may be related to the cellular volume as:

$$f_1 = V_1/V_C \quad ; \quad f_2 = V_2/V_C = 1 - f_1. \tag{5}$$

In this way the three volumes occupied by the EC and the different cell types may be related to the total volume by:

$$V_{EC} = \varepsilon V_T \quad ; \quad V_1 = f_1(1-\varepsilon)V_T \quad ; \quad V_2 = (1-f_1)(1-\varepsilon)V_T. \tag{6}$$

At the subcellular scale, the Fickian transmembrane transport scales with the intrinsic transmembrane concentration difference. A sub-domain's intrinsic concentration is a volume averaged mass concentration in which the drug mass stored in a sub-domain is averaged only over the volume of that subdomain. Because in this study there are no transient or spatial variations in the subdomain

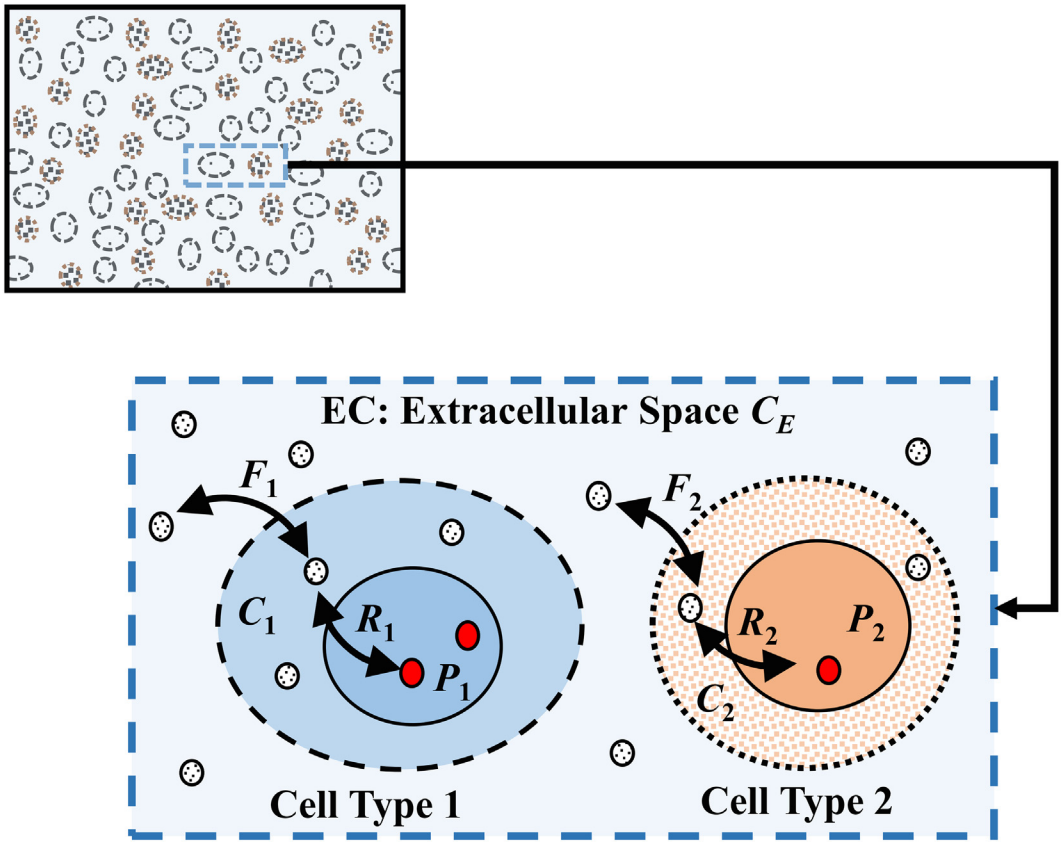

Fig. 2. Conceptual depiction of drug delivery to a tissue composed of a two-cell-type population.

volumes in Eq. (6), the intrinsic concentrations may be simply represented as the ratio of the drug mass of each subdomain to that subdomain's volume:

$$C_{EC} = \frac{m_{EC}}{V_{EC}} \quad ; \quad C_1 = \frac{m_1}{V_1} \quad ; \quad C_2 = \frac{m_2}{V_2}. \tag{7}$$

This differs from the total volume averaged concentrations which is the mass of the drug stored in the sub-domain that is averaged over the total domain volume. Formal descriptions of the determination of the intrinsic concentration and the total volume averaged concentration is presented in Section 3.2 of the book (de Monte et al., 2013). In this study the total volume averaged concentrations simplify to the ratio of the drug mass stored in each sub-domain to the total volume:

$$\overline{C}_{EC} = \frac{m_{EC}}{V_T} \quad ; \quad \overline{C}_1 = \frac{m_1}{V_T} \quad ; \quad \overline{C}_2 = \frac{m_2}{V_T}. \tag{8}$$

Here the total volume is $V_T = V_{EC} + V_1 + V_2$. Substituting (6) and (8) into (7), the total volume averaged concentration may be related to their intrinsic counterparts by the expressions:

$$\begin{aligned} \overline{C}_{EC} &= C_{EC} \cdot \varepsilon \\ \overline{C}_1 &= C_1 \cdot f_1 \cdot (1-\varepsilon) \\ \overline{C}_2 &= C_2 \cdot (1-f_1) \cdot (1-\varepsilon). \end{aligned} \tag{9}$$

2.2. Governing equations: application to the tumor chord

A first principles derivation of the set of equations governing mass transfer of the three compartment model of two cell types is provided in Appendix A. In the study that follows, the governing equations are applied to an axi-symmetric cylindrical region of tissue surrounding a small blood vessel representative of a tumor chord. The tissue is situated within the radial coordinates $r_I \leqslant r \leqslant r_O$ where r_I is the radial position of the vessel-tissue interface and r_O is the radial position at the outer boundary of the domain. This is depicted in Fig. 3.

In the following analysis, the reaction terms of both cell types are equal to one another and are represented by a reversible saturable binding model similar to that presented in (Groh et al., 2014; Clarelli et al., 2020) for which:

$$R_i = k_1 C_i (C_0 - P_i) - k_{-1} P_i \quad i = 1, 2. \tag{10}$$

Here the index i refers to cell type number. The parameter C_0 is the limiting binding site concentration within the intracellular space. Its value limits the binding rate at "saturation". The parameter k_1 is the drug association rate, and k_{-1} is the drug disassociation rate.

In this study, the mass transfer in the extracellular space is described by simple diffusion, so that the axi-symmetric coupled set of equations governing the conservation of drug mass is:

$$\begin{aligned} \frac{\partial}{\partial t}(C_{EC}) &= D\left[\frac{\partial^2}{\partial r^2}(C_{EC}) + \frac{1}{r}\frac{\partial}{\partial r}(C_{EC})\right] \\ &\quad - \frac{(1-\varepsilon)}{\varepsilon} f_1 \mu_1 (C_{EC} - C_1) - \frac{(1-\varepsilon)}{\varepsilon}(1-f_1)\mu_2 (C_{EC} - C_2) \\ \frac{\partial}{\partial t}(C_1) &= \mu_1 (C_{EC} - C_1) - k_1 C_1 (C_0 - P_1) + k_{-1} P_1 \\ \frac{\partial}{\partial t}(C_2) &= \mu_2 (C_{EC} - C_2) - k_1 C_2 (C_0 - P_2) + k_{-1} P_2. \end{aligned} \tag{11}$$

Here the parameters μ_1 and μ_2 are the mass transfer coefficients associated with Cell Type 1 and Cell Type 2 respectively. Their magnitudes are proportional to the permeability to the drug of the cell different membrane types. Because the EC is a porous

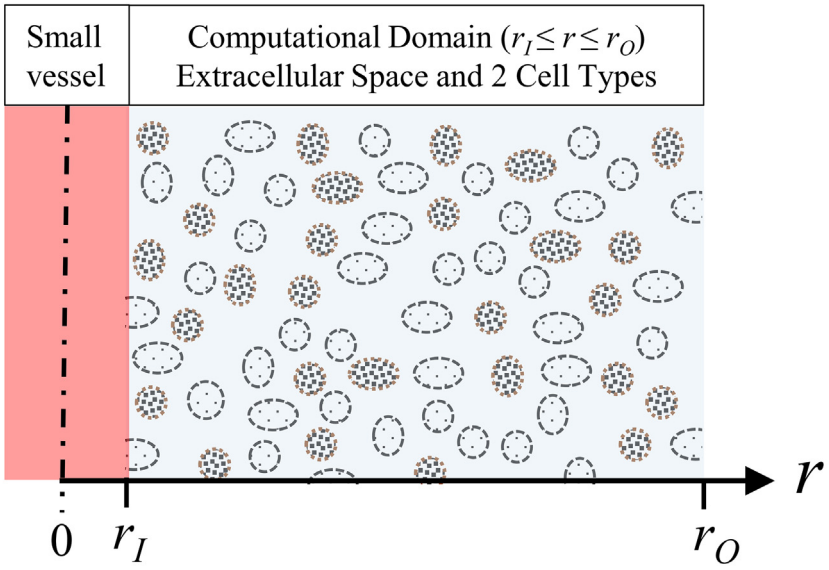

$$r = r_I: \quad D\frac{\partial C_{EC}}{\partial r} = h\left(C_p - C_{EC}\right) \qquad r = r_O: \quad \frac{\partial C_{EC}}{\partial r} = 0$$

Fig. 3. Depiction of the computational domain representing a tumor chord that is composed of two cell types and that surrounds a small blood vessel.

domain, an effective diffusion coefficient, D, is used to account for the tortuous pathway through the fluid filled space. The rate at which the product of reaction occurs in each cell type is represented by:

$$\frac{\partial}{\partial t}(P_1) = k_1 C_1 (C_0 - P_1) - k_{-1} P_1$$
$$\frac{\partial}{\partial t}(P_2) = k_1 C_2 (C_0 - P_2) - k_{-1} P_2. \tag{12}$$

2.3. Initial conditions and boundary conditions.

Equations (11)–(12) are subject to the following homogeneous initial conditions:

$$t = 0: \ C_{EC} = C_1 = C_2 = P_1 = P_2 = 0 \qquad \text{in } r_i \leqslant r \leqslant r_O, \tag{13}$$

At the outer boundary, a no flux condition is imposed in the EC:

$$r = r_O: \quad \frac{\partial C_{EC}}{\partial r} = 0. \tag{14}$$

A case study is conducted based on the one presented in (Groh et al., 2014) in which the drug is injected into the blood stream so that it enters the EC at the tissue-vessel interface. This infusion mediated delivery is represented using a type III boundary condition at the tissue-vessel interface:

$$t \geqslant 0, \quad r = r_I: \quad D\frac{\partial C_{EC}}{\partial r} = h(C_p - C_{EC}). \tag{15}$$

Here h is the permeability of the vessel wall to the drug and the concentration of the drug in the plasma is represented by a mono-exponentially decaying pharmacokinetic profile (Groh et al., 2014):

$$C_p = a \cdot \exp(-t/\tau). \tag{16}$$

2.4. Numerical modeling considerations

Equations (11) and (12) subject to Boundary and Initial Conditions (14)-(16) were evaluated numerically in the commercially available software COMSOL 5.5. In the EC, the drug concentration was solved using the Transport of Diluted Species Solver of the Chemical Species Module. For each of the remaining concentrations and products of reactions, a Domain ODE and DAEs solver of the Mathematics module was used. These equations were time integrated using the inbuilt implicit backwards differentiation formula (BDF) solver set at a maximum order of 2. By default, the software uses an adaptive time step and in this study the maximum allowable time step was limited to Δt_{max} = 1 s. The radial domain

Table 1
Parameter descriptions and values used in this study. With the exception of the drug resistive cell permeability, μ_1, and the geometry, all parameters have been determined from those of (Groh et al., 2014).

Symbol	Parameter	Value	Used in Eq.
D	Effective Extracellular Drug Diffusion Coefficient	7.5×10^{-10} $m^2 s^{-1}$	(11), (15)
ε	Tissue Porosity	1/17	(11)
μ_1	Drug Resistive Cell Membrane Permeability	4.123×10^{-3} s^{-1}	(11)
μ_2	Drug Receptive Cell Membrane Permeability	0.2062 s^{-1}	(11)
C_0	Intracellular Binding Saturation Concentration	2.6×10^3 μM	(11), (12)
k_1	Drug Association Rate Constant	9×10^{-7} $\mu M^{-1} s^{-1}$	(11), (12)
k_{-1}	Drug Disassociation Rate Constant	1.4×10^{-5} s^{-1} [a]	(11), (12)
r_I	Radial Location of Tissue – Vessel Interface	20 μM	(13), (14), (15)
r_O	Outer Radial Position of Domain Boundary	10^3 μM	(13), (14), (15)
h	Vessel-Tissue Permeability to the Drug	2.125×10^{-6} m s^{-1}	(15)
a	Initial Infusion Concentration at the Vessel Wall	50 μM	(16)
τ	Infusion Concentration Decay Constant	200 s	(16)

[a] The drug dissacociation rate constant is taken from the electronic supplementary material of (Groh et al, 2014)

was discretized using uniform grid length of Δr = 1.96 μm resulting in 500 nodes. The choices in times step restriction and grid size were informed by a resolution study that is presented in Appendix B1.

This study is conducted within the radial coordinates: $r_l = 20\,\mu m$ and $r_o = 10^3\,\mu m$. Cell Type 1 is very resistive to the drug and is assigned a mass transfer coefficient of $\mu_1 = 4.123 \times 10^{-3}$ s^{-1} this value is 50 times smaller than the mass transfer coefficient of Cell Type 2 , $\mu_2 = 0.2062$ s^{-1} which is representative of the experimentally determined permeability of the membranes of tumor cells to DOX reported in (Groh et al., 2014). The remaining parameter values are also determined from those presented in (Groh et al., 2014) which are representative of the infusion mediated delivery of DOX to tumor cells surrounding a small vessel and are summarized in Table 1. Note that the supplementary electronic material of (Groh et al., 2014) presents a drug disassociation rate constant, k_{-1}, that is one order of magnitude smaller than that reported in the main article; this study uses the smaller value.

The numerical solution method of the current study has been verified in a comparison with the published single cell population study of (Groh et al., 2014). Quantitative comparisons are presented in Appendix B and the numerical results at specified times and radial locations are in excellent agreement with the published values. This also re-enforces the chosen drug disassociation rate constant.

In the study that follows the delivery of the drug to the tumor chord by infusion from the vessel is modeled. The tumor chord is composed of 2 cell types for which the membrane of one cell type is much less permeable to the drug than the other cell type. Two different cell populations are studied: in one, most of the population is composed of drug impermeable cell type (f_1 = 0.9), and in the other case most of the population is composed of drug permeable cell types (f_1 = 0.1).

3. Results and discussion

The purpose of this work is to model the delivery of drugs to cells in tissue for which the tissue is composed of two different cell types. It has been shown experimentally that one of the contributing factors to drug resistance in cells is related to the permeability of the drug in the cell membrane. Here we consider the case when the permeability of Cell Type 1 is 50 times lower than that of Cell Type 2. Two different types of cell population are considered: a population that is composed of 10% of the drug resistant Cell Type 1 (f_1 = 0.1) and a second population that is composed of 90% of the drug resistant Cell Type 1 (f_1 = 0.9).

The spatial distribution of the product of reaction at a time one hour after the beginning of the drug administration for these two different population compositions are considered first. The concentration of the products of reaction of both cell types decrease in exponentially with distance from the vessel wall regardless of population composition (Fig. 4a). The concentration profiles of the product of reaction of the drug resistant cells, P_1 are consistently lower than those associated with the less resistive cells, P_2 . At all locations, the both cell types exhibit lower conentrations of products of reaction when the population is composed of drug permeable cells compared to when the population is composed mostly of drug resistant cells. The transient profiles at r = 0.25 μm (Fig. 4b) reveal that for both population types, the peak conentration of the product of reaction occurs within 30 minutes and that the peak values of both cell types decseases as more of the population is composed of the drug permeable cells.

The reason that the reaction within the cell is strongly influenced by the composition of the population can be explained by looking at the transient drug concentration in each cell type and the transient concentration of the drug in the EC.

The influence of population composition on the resulting transient concentration profiles at r = 25 μm are plotted in Fig. 5. At this location, the intracellular drug concentrations of the drug resistant Cell Type 1 (Fig. 5a blue lines) and of the drug permeable Cell Type 2 (Fig. 5a red lines) are both affected by population composition. This sensitivity can be explained as follows. When the resistant Cell Type 1 makes up a small proportion of the cell population (f = 0.1) a greater volume of the tissue is composed of the higher permeability Cell Type 2. The rate that the EC is depleted of the drug increases with the fraction of the population composed of the permeable cells (with decreasing f_1). This population dependence of the depletion is evident in the transient extracellular drug concentration profile (Fig. 5b). Because rate of drug uptake is proportional to the transmembrane concentration difference (Eq. (11)) and because for low f_1 there is simply less drug available in the EC (Fig. 5b), the resistive Cell Type 1 experiences slower drug uptake (and hence lower values C_1) for lower values of f_1; there is less drug available to experience the intracellular drug reaction of Eq. (10) and this results in the inverse dependence of P_1 on f_1 observed in Fig. 4.

The transient behavior of the concentrations at a location farther away from the vessel-tissue interface, at r = 150 μm, have been plotted in Fig. 6. At this location, the intracellular drug con-

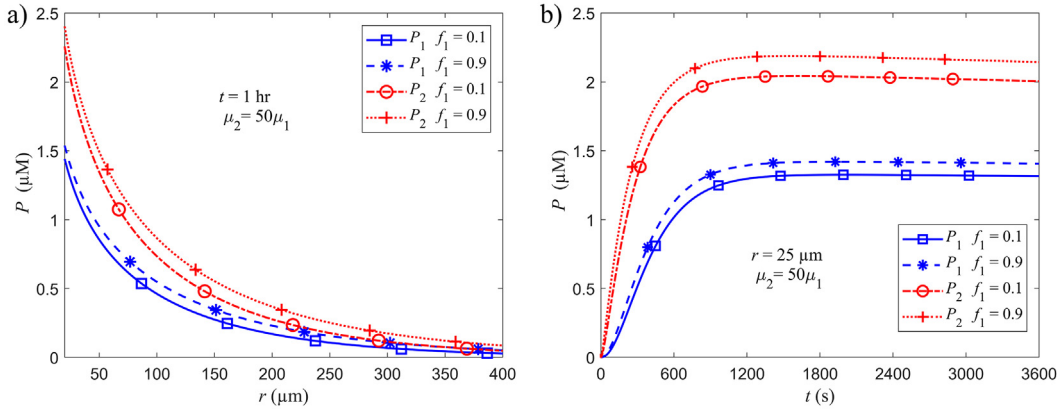

Fig. 4. The concentration of the product of reaction of resistive Cell Type 1 (blue lines) and responsive Cell Type 2 (red lines) ofor: a) the spatial profiles one hour post drug administration and b) the transient profiles at r = 25 μm. Here the population composition is either 10% or 90% of Cell Type 1 (f_1) and the permeability of Cell Type 1 is 1/50 that of Cell Type 2.

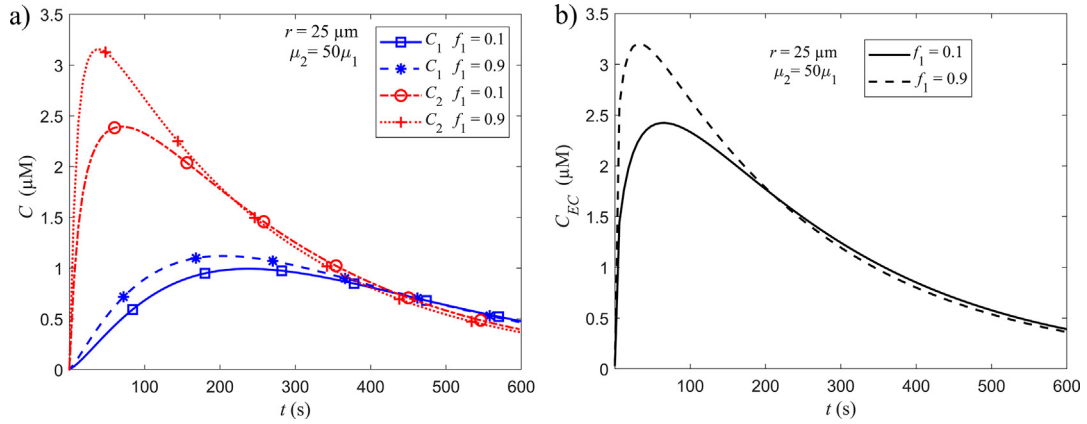

Fig. 5. The transient behavior at r = 25 μm of: a) the intracellular concentrations of both Cell Type 1 (blue lines) and Cell Type 2 (red lines) and b) the extracellular concentration. Here the population composition is either 10% or 90% of Cell Type 1 (f_1) and the permeability of Cell Type 1 is 1/50 that of Cell Type 2.

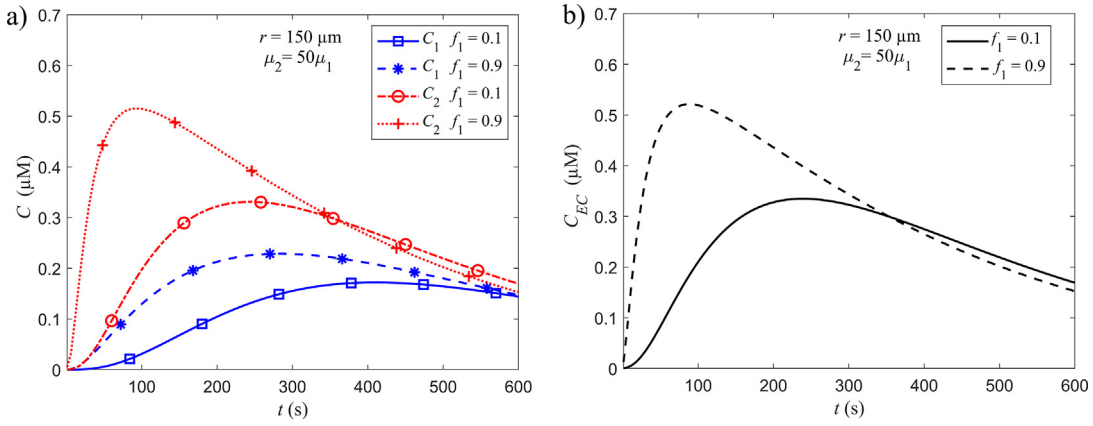

Fig. 6. The transient behavior at r = 150 μm of a) the intracellular concentrations of Cell Type 1 (blue lines) and Cell Type 2 (red lines) and of b) the of the extracellular concentration. Here the population composition is either 10% or 90% of Cell Type 1 (f_1) and the permeability of Cell Type 1 is 1/50 that of Cell Type 2.

centrations (Fig. 6a) of both Cell Type 1 (blue lines) and Cell Type 2 (red lines) increase with increasing f_1. Recalling Eq. (12), the lower intracellular drug concentrations are anticipated to result in the in lower production rates of P_1 and P_2 and this is reflected in the profiles of Fig. 4 at r = 150 μm. When the more permeable Cell Type 2 makes up a large proportion of the cell population (f_1 = 0.1), the EC at locations closer to the vessel wall is depleted of the drug (Fig. 4b). The diffusive transport within the EC depends on the extracellular concentration gradient and this gradient decreases with the previously described depletion that occurs near the vessel-tissue interface at low f_1. Thus less drug is transported to regions farther away from the vessel-tissue interface (Fig. 6b). With low values of f_1, there is simply less drug available in the EC at higher radial positions. Because the rate of drug uptake into both cell types is proportional to the transmembrane concentration differences, lower values of C_{EC} result in less drug uptake and hence the lower values of P_1 and P_2 seen in Fig. 4.

4. Conclusions

The models reviewed in this paper that do capture the continuum dynamic behavior of drug mass in cell cultures or in tissues all considered a population composed of only a single cell type. This has obvious limitations when, for example, a drug is delivered to tissue composed of different types of cells that react very differently to a drug. There are some existing models of multiple–cell–type population in applications such as viral dynamics, tumor growth, and cell chemotaxis. However, these models do not conserve the drug (or chemical species); instead these focus on the conservation of the transient cell density of the different cell types. The model presented in this study allows researchers to predict the drug uptake by a population composed of different cell types which has the potential to be especially useful in the prediction of the efficacy of treatments when the tissues or cell cultures are heterogeneous.

The three compartment pharmacokinetic model of drug delivery to tissues has been extended to represent tissue composed of two different cell types. A first principles derivation of the model is presented and the numerical method is quantitatively verified in a comparison with a published study of drug delivery to tissue composed of a single–cell–type. A case study is presented of a population composed of two cell types that are distinguished by their transmembrane drug permeability values. The two–cell–type population model is used to determine the influence of population composition on delivery of drugs to tissues surrounding a small blood vessel. When the cell population of the tissue is composed primarily of drug permeable cells, the drug concentration within the EC is quickly depleted. This leads to lower values of drug uptake and metabolic reaction by drug resistant cells (compared to the case when the tissue is composed primarily of drug resistant cells). At regions farther away from the blood vessel (∼4 vessel diameters) increasing the fraction of cells that are permeable to

the drug results in lower values of intracellular drug concentration and metabolism for both cell types.

CRediT authorship contribution statement

Sid Becker: Writing – original draft, Conceptualization, Methodology, Validation, Software, Visualization, Formal analysis, Writing – review & editing. **Andrey V. Kuznetsov:** Conceptualization, Methodology, Writing – review & editing. **Dan Zhao:** Conceptualization, Methodology, Writing – review & editing. **Filippo de Monte:** Conceptualization, Writing – original draft, Writing – review & editing. **Giuseppe Pontrelli:** Conceptualization, Writing – original draft.

Declaration of Competing Interest

The authors declare that they have no known competing financial interests or personal relationships that could have appeared to influence the work reported in this paper.

Acknowledgment

Giuseppe Pontrelli acknowledges funding from the European Research Council under the European Unions Horizon 2020 Framework Programme (No. FP/2014–2020)/ ERC Grant Agreement No. 739964 (COPMAT).

Appendix A. Derivation of the governing equations

Consider an elementary control volume (CV) of total volume is $V_T = \Delta x \Delta y \Delta z$ as depicted in Fig. 7. If the porosity of the CV is uniform, each of the control volume faces have equal areas occupied by the EC. The area in the *y-z* plane that is occupied by the EC is A_{EC} and this is treated here as a constant.

All transmembrane mass transfer (for both cell types) is represented as a Fickian process *across the cell membrane* so that the drug transport is proportional to the difference in the intrinsic drug concentrations on either side of the cell wall. The membranes of the different cell types may have different resistances to mass transfer. Within this CV, the rate of drug mass uptake by each cell type is also proportional to the total number of cells of that type (volume occupied by cells of that type within the CV). With that in mind and following the derivations presented in (Boyd and Becker, 2016; Argus et al., 2017; Mahnic-Kalamiza et al., 2014), the transport of mass into each of the cell domains are represented as follows. The net rate of mass uptake into the volumes occupied by the different cell types resulting from the transport across the cell membranes are:

$$\begin{aligned} \dot{m}_1 &= \mu_1(C_{EC} - C_1)V_1 \\ \dot{m}_2 &= \mu_2(C_{EC} - C_2)V_2 \end{aligned}. \tag{A1}$$

Here the subscripted parameter, μ, is the mass transfer coefficient. Its magnitude reflects the permeability of the cell membrane to the drug. Within each cell type, a chemical reaction consumes (or binds) the free drug. The time rate change of drug mass stored in the volume occupied by each cell type is increased by the net rate of drug mass entering the cell types and is decreased by the reaction. Thus the rate of drug mass stored in each of the cell types is represented:

$$\begin{aligned} \frac{\partial}{\partial t}(m_1) &= \mu_1(C_{EC} - C_1)V_1 - R_1(C_1)V_1 \\ \frac{\partial}{\partial t}(m_2) &= \mu_2(C_{EC} - C_2)V_2 - R_2(C_2)V_2, \end{aligned} \tag{A2}$$

Here the reaction rate within the cell types are represented by the general expressions $R_1(C_1)$ and $R_2(C_2)$.

The net rate of the change in mass stored within the extracellular space (m_{EC}) is decreased by the net transfer of mass leaving the CV and entering neighboring CV's and is reduced with mass uptake by each of the two cell types.

$$\frac{\partial}{\partial t}(m_{EC}) = -\dot{m}_J - \dot{m}_1 - \dot{m}_2. \tag{A3}$$

Here $\dot{m}_J$ is the net mass transfer of the drug across the CV boundaries; while this could be a result of diffusion and of advection from an interstitial flow, only diffusion is considered here. In the derivation that follows, the rate of mass in the EC that crosses the CV boundaries in the *y-z* planes is presented explicitly, and this may be extended to the other planes as well. Referring to Fig. 7 the area of the *y-z* planes of the control volume that are made up of EC space is A_{EC}. Within the EC, the net rate of mass flux leaving the CV is related to the rate of mass transfer per unit area, $\dot{m}_x''$, by the relation:

$$\dot{m}_{J,X} = \frac{\partial}{\partial x}\left(\dot{m}_x'' A_{EC}\right)\Delta x. \tag{A4}$$

The rate of mass flux is governed by diffusion only so that:

$$\dot{m}_x'' = -D\frac{\partial}{\partial x}(C_{EC}), \tag{A5}$$

where D is the effective diffusion coefficient. Substituting (A5) into (A4) and assuming homogeneous parameter values results in:

$$\dot{m}_{J,X} = -D\frac{\partial^2}{\partial x^2}(C_{EC})A_{EC}\Delta x. \tag{A6}$$

By applying the steps (A4)–(A5) to the remaining coordinate directions (or simply representing the flux with the Laplacian operator), (A6) may be represented in a more general form as:

$$\dot{m}_J = -D\nabla^2(C_{EC})A_{EC}\Delta x. \tag{A7}$$

Noting that for this CV, $A_{EC}\Delta x = V_{EC}$ and substituting (A2) and (A7) into (A3) results in:

$$\frac{\partial}{\partial t}(m_{EC}) = D\nabla^2(C_{EC})V_{EC} - \mu_1(C_{EC} - C_1)V_1 - \mu_2(C_{EC} - C_2)V_2. \tag{A8}$$

Substituting the definitions of the intrinsic concentrations of Eq. (7) and the relations of the different volumes of Eq. (6) into Eqs. (A2) and (A8) and rearranging results in the coupled system of equations:

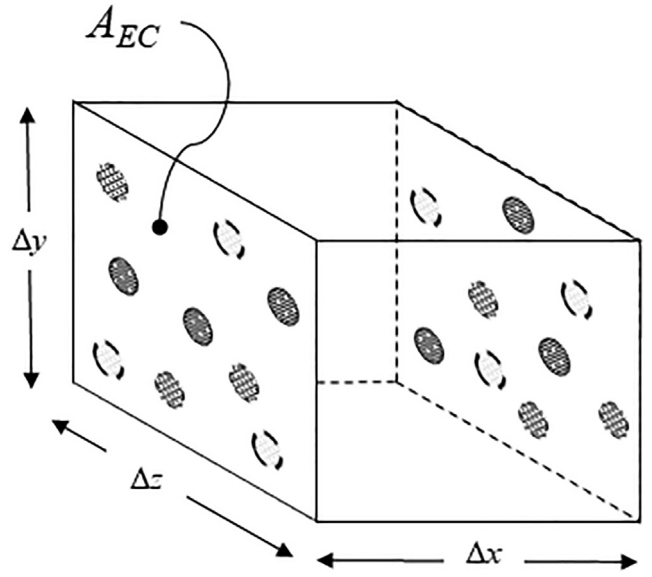

Fig. 7. A representative control volume of dimensions $\Delta x \times \Delta y \times \Delta z$ of a population composed of two different cell types for which the cell distribution is constant and homogenous.

$$\frac{\partial}{\partial t}(C_{EC}) = D\frac{\partial^2}{\partial x^2}(C_{EC}) - \frac{(1-\varepsilon)}{\varepsilon}f_1\mu_1(C_{EC}-C_1) - \frac{(1-\varepsilon)}{\varepsilon}(1-f_1)\mu_2(C_{EC}-C_2)$$
$$\frac{\partial}{\partial t}(C_1) = \mu_1(C_{EC}-C_1) - R_1(C_1)$$
$$\frac{\partial}{\partial t}(C_2) = \mu_2(C_{EC}-C_2) - R_2(C_2). \quad \text{(A9)}$$

Even though Eq. (A9) was developed and presented in Cartesian coordinates, the expression is easily represented in any coordinate system with the appropriate Laplacian operator. The rate at which the product of reaction in each cell type is represented as:

$$\frac{\partial}{\partial t}(P_1) = R_1(C_1)$$
$$\frac{\partial}{\partial t}(P_2) = R_2(C_2). \quad \text{(A10)}$$

Appendix B. Method verification

Spatio-Temporal resolution

Grid size and timestep resolution studies have been conducted in the numerical integration of Eqs.(10) – (16). The local magnitudes of the concentration product of reaction in cell type 2 at 600 s, $P_2(r, 600\text{s})$, for a population of cells for which f_1 = 0.9, are evaluated in the following comparisons.

In the grid refinement study, 4 simulations were conducted with different numbers of nodes, N, placed at regularly spaced radial intervals. Solutions of different grid sizes were compared to a very refined mesh: $N = 10^4$ at grid spacing of $\Delta r = 9.8 \times 10^{-2}$ μm. All used the same maximum allowable timestep of 1 s. The local absolute percent difference between the solution of a grid of node number, N, compared to a the very refined mesh of $N = 10^4$ is defined as:

$$\delta_x \equiv 100 \times \left|1 - \frac{P_2(r, t = 600\text{ s}, N)}{P_2(r, t = 600\text{ s}, N = 10,000)}\right|. \quad \text{(B1)}$$

The local percent differences for N = 100, 500, and 1000 are plotted over the computational domain at t = 600 s in Fig. 8a. The mesh that was used to develop the results of Section 3 corresponds to N = 500 nodes equally spaced at intervals of Δr = 1.96 μm; in this case the absolute percent difference with the very refined mesh is never above 0.01%.

A time step sensitivity analysis was conducted in which time integrations using the BDF solver were carried out at different maximum allowable time steps Δt_{max} = 10, 1, 0.1, and 0.001 s.

Table B1
Comparison with the results published in (Groh et al., 2014).

Location and time	C_{EC} (μM)		P_1 (μM)	
	(Groh et al., 2014)	This Study (% diff.)	(Groh et al., 2014)	This Study (% diff.)
26 μm, 75 s	1.80	1.84 (2.2%)		
108 μm, 265 s	0.523	0.515 (−1.5%)		
190 μm, 374 s	0.406	0.399 (−1.7%)		
26 μm, 0:41:02 (h:m:s)			1.93	1.96 (1.6%)
108 μm, 1:02:28 (h:m:s)			0.983	0.971 (−1.2%)
190 μm, 31:45:39 s (h:m:s)			0.872	0.860 (−1.4%)

The local absolute percent difference of the solutions (compared to the very refined time step) is defined as:

$$\delta_t \equiv 100 \times \left|1 - \frac{P_2(r, t = 600\text{ s}, \Delta t_{max})}{P_2(r, t = 600\text{ s}, \Delta t_{max} = 0.01\text{ s})}\right|. \quad \text{(B2)}$$

The local percent differences for Δt_{max} = 10, 1, and 0.1 s are plotted over the computational domain at t = 600 s in Fig. 8b. The maximum allowable time step that was used to develop the results of Section 3 corresponds to Δt_{max} = 1 s; in this case the absolute percent difference is always below 0.001%.

Solution method verification

To verify the numerical methodology used in the current study, a comparison is made to the results of (Groh et al., 2014) which considers the delivery of DOX to in a radially symmetric tumor situated around a blood vessel. In that study the reaction is represented by a reversible saturable binding model so that the drug conservation within the single–cell–type population is governed by:

$$\frac{\partial}{\partial t}(C_{EC}) = D\left[\frac{\partial^2}{\partial r^2}(C_{EC}) + \frac{1}{r}\frac{\partial}{\partial r}(C_{EC})\right] - \frac{(1-\varepsilon)}{\varepsilon}\mu(C_{EC}-C_1)$$
$$\frac{\partial}{\partial t}(C_1) = \mu(C_{EC}-C_1) - k_1C_1(C_0-P_1) + k_{-1}P_1$$
$$\frac{\partial}{\partial t}(P_1) = k_1C_1(C_0-P_1) - k_{-1}P_1. \quad \text{(B3)}$$

This is subject to the following homogeneous initial conditions:

$$t = 0: \; C_{EC} = C_1 = P_1 = 0 \qquad \text{in } r_I \leqslant r \leqslant r_O, \quad \text{(B4)}$$

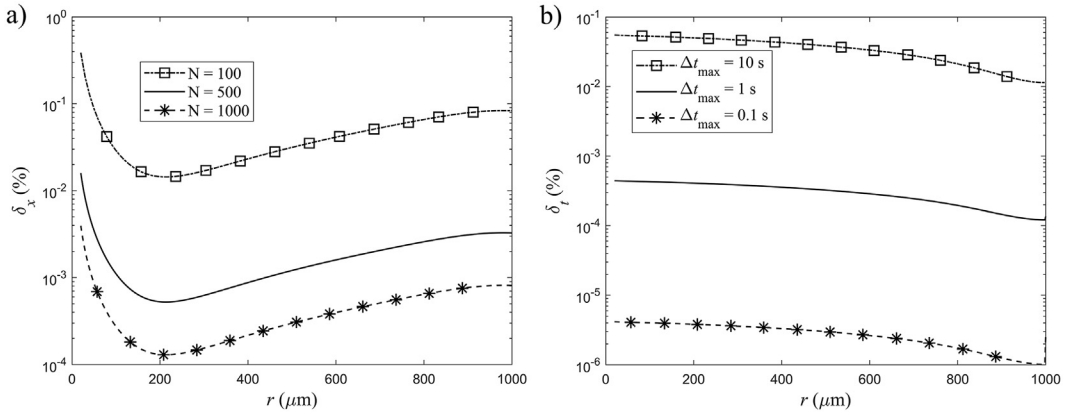

Fig. 8. Spatio-temporal refinement comparisons of absolute percent difference in the solutions to the product of reaction in the drug receptive cell type in a population with f_1 = 0.1 at 600 s for: a) a mesh refinement at different number of nodes compared to a very refined mesh of 10,000 nodes as defined by Eq. (B1), and b) a time step refinement at different maximum allowable time steps compared to the Δt_{max} = 0.01 s as defined by Eq. (B2).

and the EC is subject to a type III boundary transient boundary condition at the tumor-vessel interface and a no flux condition at the outer boundary:

$$D\frac{\partial}{\partial r}(C_{EC})\Big|_{r_I} = h(C_p - C_{EC})\frac{\partial}{\partial r}(C_{EC})\Big|_{r_O} = 0. \quad \text{(B5)}$$

The concentration of the drug in the plasma is represented by a mono-exponentially decaying pharmacokinetic profile:

$$C_p = a \cdot \exp(-t/\tau), \quad \text{(B6)}$$

Simulations are conducted using the paramteter values of (Groh et al., 2014) for which: r_I=16 μm, r_O=200 μm, μ=0.2062 s^{-1}, and the remaining are those listed in Table 1.

In this comparison study, the concentration in the EC and the concentration of the product of reaction in the intracellular space are considered at the three radial positions: 16 μm, 108 μm, and 190 μm. The maximum values of the product of reaction and the extracellular concentration at these locations and the time at which these maximum concentrations are reached published in (Groh et al., 2014). Concentration values at these locations and times are determined numerically in the current study and side by side comparisons are presented in Table B1. The current study values are in very good agreement with the published results. Note that because the simulations include times up to 31.75 h, the grid resolution was set to N = 100 with COMSOL's default unconstrained adaptive time stepping BDF method.

References

Aminipour, Z., Khorshid, M., Keshvari, H., Bonakdar, S., Wagner, P., Van der Bruggen, B., 2020. Passive permeability assay of doxorubicin through model cell membranes under cancerous and normal membrane potential conditions. Eur. J. Pharm. Biopharm. 146, 133–142.

Argus, F., Boyd, B., Becker, S.M., 2017. Electroporation of tissue and cells: A three-equation model of drug delivery. Computers Biology Med. 84, 226–234.

Bell, C., Hill, C., Burton, C., Blanchard, A., Shephard, F., Rauch, C., 2013. Importance of the Difference in Surface Pressures of the Cell Membrane in Doxorubicin Resistant Cells That do not Express Pgp and ABCG2. Cell Biochem. Biophys. 66 (3), 499–512.

Bocharov, G.A., Volpert, V.A., Tasevich, A.L., 2018. Reaction-Diffusion Equations in Immunology. Comput. Math. Math. Phys. 58 (12), 1967–1976.

Boyd, B. and S. Becker, Macroscopic Modeling of In Vivo Drug Transport in Electroporated Tissue. Journal of Biomechanical Engineering, 2016. **138**(3): p. 031008-031008-11.

Breward, C.J.W., Byrne, H.M., Lewis, C.E., 2002. The role of cell-cell interactions in a two-phase model for avascular tumour growth. J. Math. Biol. 45 (2), 125–152.

Byrne, H.M., King, J.R., McElwain, D.L.S., Preziosi, L., 2003. A two-phase model of solid tumour growth. Appl. Math. Lett. 16 (4), 567–573.

Casciari, J.J., Sotirchos, S.V., Sutherland, R.M., 1992. Mathematical modelling of microenvironment and growth in EMT6/Ro multicellular tumour spheroids. Cell Prolif. 25 (1), 1–22.

Chakravarty, K., Dalal, D.C., 2019. A Nonlinear Mathematical Model of Drug Delivery from Polymeric Matrix. Bull. Math. Biol. 81 (1), 105–130.

Clarelli, F., Liang, J., Martinecz, A., Heiland, I., Abel zur Wiesch, P., 2020. Multi-scale modeling of drug binding kinetics to predict drug efficacy. Cellular Molecular Life Sci.: CMLS 77 (3), 381–394.

de Monte, F., Pontrelli, G., Becker, S., 2013. Chapter 3 - Drug Release in Biological Tissues. In: Transport in Biological Media. Elsevier, Boston, pp. 59–118.

Dordal, M.S., Ho, A.C., Jackson-Stone, M., Fu, Y.F., Goolsby, C.L., Winter, J.N., 1995. Flow cytometric assessment of the cellular pharmacokinetics of fluorescent drugs. Cytometry (New York, N.Y.) 20 (4), 307–314.

Eikenberry, S., A tumor cord model for doxorubicin delivery and dose optimization in solid tumors. Theor. Biol. Med., 2009. **6**(1): p. 16-16.

El-Kareh, A.W. and T.W. Secomb, A Mathematical Model for Comparison of Bolus Injection, Continuous Infusion, and Liposomal Delivery of Doxorubicin to Tumor Cells1. Neoplasia (New York, N.Y.), 2000. **2**(4): p. 325-338.

Ferté, J., 2000. Analysis of the tangled relationships between P-glycoprotein-mediated multidrug resistance and the lipid phase of the cell membrane. Eur. J. Biochem. 267 (2), 277–294.

Flegg, J.A., Nataraj, N., 2019. Mathematical Modelling and Avascular Tumour Growth: Interdisciplinary Research. Resonance 24 (3), 313–325.

Groh, C.M., Hubbard, M.E., Jones, P.F., Loadman, P.M., Periasamy, N., Sleeman, B.D., Smye, S.W., Twelves, C.J., Phillips, R.M., 2014. Mathematical and computational models of drug transport in tumours. J. R. Soc. Interface 11 (94), 20131173. https://doi.org/10.1098/rsif.2013.1173.

Hillen, T., Painter, K.J., 2009. A user's guide to PDE models for chemotaxis. J. Math. Biol. 58 (1-2), 183–217.

Horstmann, D., 1970. From 1970 Until Present: the Keller-Segel Model in Chemotaxis and Its Consequences. Niedersächsische Staats- und Universitätsbibliothek, 2003.

Lauffenburger, D.A., Linderman, J.J., 1993. Receptors: models for binding, trafficking, and signaling. Oxford University Press, New York.

Jackson, T.L., Byrne, H.M., 2000. A mathematical model to study the effects of drug resistance and vasculature on the response of solid tumors to chemotherapy. Math. Biosci. 164 (1), 17–38.

Jackson, T.L., 2003. Intracellular Accumulation and Mechanism of Action of Doxorubicin in a Spatio-temporal Tumor Model. J. Theor. Biol. 220 (2), 201–213.

Keller, E.F., Segel, L.A., 1971. Model for chemotaxis. J. Theor. Biol. 30 (2), 225–234.

Mahnic-Kalamiza, S., Miklavcic, D., Vorobiev, E., 2014. Dual-porosity model of solute diffusion in biological tissue modified by electroporation. Biochimica Et Biophysica Acta-Biomembranes 1838 (7), 1950–1966.

McGinty, S., Pontrelli, G., 2016. On the role of specific drug binding in modelling arterial eluting stents. J. Math. Chem. 54 (4), 967–976.

Meghdadi, N., Soltani, M., Niroomand-Oscuii, H., Ghalichi, F., 2016. Image based modeling of tumor growth. Australas. Phys. Eng. Sci. Med. 39 (3), 601–613.

Nowak, M.A., et al., Viral Dynamics in Hepatitis B Virus Infection. Proceedings of the National Academy of Sciences - PNAS, 1996. **93**(9): p. 4398-4402.

Painter, K.J., Maini, P.K., Othmer, H.G., 2000. Development and applications of a model for cellular response to multiple chemotactic cues. J. Math. Biol. 41 (4), 285–314.

Painter, K.J., Sherratt, J.A., 2003. Modelling the movement of interacting cell populations. J. Theor. Biol. 225 (3), 327–339.

Peetla, C., Bhave, R., Vijayaraghavalu, S., Stine, A., Kooijman, E., Labhasetwar, V., 2010. Drug Resistance in Breast Cancer Cells: Biophysical Characterization of and Doxorubicin Interactions with Membrane Lipids. Mol. Pharm. 7 (6), 2334–2348.

Preziosi, L., G. Toscani, and M. Zanella, Control of tumor growth distributions through kinetic methods. Journal of theoretical biology, 2021. **514**: p. 110579-110579.

Roose, T., Chapman, S.J., Maini, P.K., 2007. Mathematical Models of Avascular Tumor Growth. SIAM Rev. 49 (2), 179–208.

Stinner, C., Tello, J.I., Winkler, M., 2014. Competitive exclusion in a two-species chemotaxis model. J. Math. Biol. 68 (7), 1607–1626.

Vendel, E., Rottschäfer, V., de Lange, E.C.M., 2019. The need for mathematical modelling of spatial drug distribution within the brain. Fluids Barriers CNS 16 (1), 12–33.

Vendel, E., Rottschäfer, V., de Lange, E.C.M., 2019. Improving the Prediction of Local Drug Distribution Profiles in the Brain with a New 2D Mathematical Model. Bull. Math. Biol. 81 (9), 3477–3507.

Ward, J.P. and J.R. King, Mathematical modelling of avascular-tumour growth. II: Modelling growth saturation. IMA journal of mathematics applied in medicine and biology, 1999. **16**(2): p. 171-211.

Yang, N.J., Hinner, M.J., 2015. Getting across the cell membrane: an overview for small molecules, peptides, and proteins. Methods Mol. Biol. 1266, 29.

Yin, J., McCaskill, J.S., 1992. Replication of viruses in a growing plaque: a reaction-diffusion model. Biophys. J . 61 (6), 1540–1549.

Yin, A., Moes, D.J.A.R., Hasselt, J.G.C., Swen, J.J., Guchelaar, H.-J., 2019. A Review of Mathematical Models for Tumor Dynamics and Treatment Resistance Evolution of Solid Tumors. CPT: Pharmacometrics Systems Pharmacology 8 (10), 720–737.

You, L., Yin, J., 1999. Amplification and Spread of Viruses in a Growing Plaque. J. Theor. Biol. 200 (4), 365–373.